

# Negative-effective-mass ballistic field-effect transistor: Theory and modeling

Z. S. Gribnikov,<sup>a)</sup> N. Z. Vagidov, A. N. Korshak, and V. V. Mitin

*Department of Electrical and Computer Engineering, Wayne State University, Detroit, Michigan 48202*

(Received 4 October 1999; accepted for publication 15 February 2000)

We consider  $p^+pp^+$  diodes, in which the middle  $p$  region (base) consists of a  $p$ -type quantum well current-conducting channel that is controlled by a gate potential. Hole concentrations in the channel are assumed to be such that a ballistic current flows only in the lowest quantized subband. This subband contains a negative-effective-mass (NEM) section in the dispersion relation. We carry out numerical simulation for realistic designs of this ballistic field-effect transistor (FET) and compare them to simple analytical estimates. We show that three types of self-organized terahertz current oscillations appear in these FETs. Two of these types originate from the NEM instability, while the third arises from the two-stream instability, predicted before for conventional ballistic diodes and FETs. Frequencies of the NEM oscillations are controlled effectively by a gate potential. They are substantially higher than frequencies of two-stream oscillations. The NEM oscillation frequencies exceed 2.5 THz for large enhancing gate potentials. © 2000 American Institute of Physics. [S0021-8979(00)06910-3]

## I. INTRODUCTION

This article is devoted to a theoretical study of field-effect transistors (FETs) where ballistic transport occurs in a current-conducting channel. We present analytical estimates for a simplified FET model with symmetric gates on both sides of the channel [Fig. 1(a)] and numerical simulations for a more realistic model with a single top gate over the channel [Fig. 1(b)]. The basic feature of our device consists of the dispersion relation of channel current carriers, which we assume to contain a negative effective-mass (NEM) section, as shown in Fig. 2. It has been shown previously<sup>1-3</sup> that the presence of such a section leads to an instability of stationary current regimes in ballistic  $n^+nn^+$  and  $p^+pp^+$  diodes and the self-organization of oscillatory regimes with periodic current oscillations. The oscillation frequency is higher if the diode bases are shorter, and the frequency exceeds 1 THz for the base lengths shorter than 0.2  $\mu\text{m}$ . These oscillations are predicted both for bulk samples<sup>4,5</sup> and for two-dimensional (2D) electron gases (in double or combined quantum wells<sup>6</sup>) and 2D hole gases (in square  $p$ -type quantum wells<sup>5,7</sup>). Since the quantum wells (QWs) can be used as current-conducting channels of FETs, we can arrange gate control of stationary and oscillatory regimes of the ballistic generator.

The presence of a controlling gate transforms the ballistic diode into a ballistic FET. The theory of ballistic FETs for the simplest channel carrier dispersion relation  $\varepsilon(p) = p^2/2m$  (where  $p$  is a momentum,  $m$  is an effective mass) was originally developed in Refs. 8 and 9. It was shown that a current of the ballistic FET becomes saturated with increase in drain voltage  $V_D$ , and a saturated current value  $I = I_S$  is proportional to  $(V_G + V_{Go})^{3/2}$ , where  $V_G$  is a gate potential (relative to a source), and  $V_{Go}$  is determined by

initial channel carrier density. The saturation voltage  $V = V_S$  is proportional to  $V_G + V_{Go}$ . When  $V_D < V_S$ , all of the drain voltage drops across a source-adjacent region, and a quasineutral region (QR) forms over most of the channel. When  $V_D > V_S$ , the excess drain voltage ( $V_D - V_S$ ) drops across a drain-adjacent region, and now the QR is shortened by the extent of a depletion layer on the drain side. Such behavior of the ballistic FET is similar to the behavior of the ballistic NEM diode.<sup>1</sup> A current in this diode is saturated at a certain voltage  $V_c \cong \varepsilon_c/e$  (see Fig. 2), and the voltage  $V_D$  drops across a source-adjacent depletion region if  $V < V_c$ . (As the source we have in mind the cathode of the  $n^+nn^+$  diode or the anode of the  $p^+pp^+$  diode.) But if  $V_D > V_c$ , an excess voltage  $V_D - V_c$  drops, as in the previous case, across a drain-adjacent extending depletion region. The size of the saturation voltage interval in the ballistic NEM diode is bound above by value  $V_k \cong \varepsilon_k/e$  that can be obtained from Fig. 2. When  $V_D > V_k$ , the spatial charge structure reforms substantially, and the diode current increases again. The stationary current is unstable exactly in the saturation interval of voltages ( $V_c, V_k$ ), where ordered current oscillations appear instead. The oscillation frequency depends on the base length that in turn depends on the base doping and also on dispersion relation details.

We show below that the changeover to the ballistic NEM FET allows us to control not only stationary characteristics of the device but also all the parameters of the oscillatory regime using the gate potential  $V_G$ . Specifically, we can switch the current oscillations on and off, change their amplitude and (this is especially important) change their frequency in a wide range. Another useful feature of the FET is separation of stationary and oscillation currents. The unstable plasma is separated from the source by a depletion layer where an almost stationary potential distribution exists. Therefore, as in the NEM diode, an oscillation region in the NEM FET is on the right side of the channel (Fig. 1). As a

<sup>a)</sup> Author to whom correspondence should be addressed; electronic mail: zinovi@ciao.eng.wayne.edu

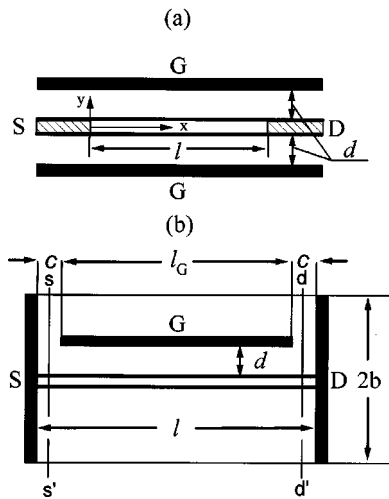


FIG. 1. Considered designs of field-effect transistors. (a) Symmetrical double-gate design selected for analytic consideration. (b) Asymmetrical periodic single-gate design selected for numerical simulation. Planes  $ss'$  and  $dd'$  are planes in which source and drain full currents are calculated. Source, drain, and gate are denoted as S, D, and G, respectively.

result of such positioning almost all of the oscillatory current flows in the gate-drain circuit. The stationary current, on the other hand, flows between source and drain since the QW barrier is assumed to be nonconducting. Generally speaking, this separation of currents allows us to choose source contact materials and schemes of source injection of hot ballistic carriers<sup>10</sup> with great flexibility.

The article is organized as follows. In Sec. II we remind readers of the basic results on ballistic transport in doped diode structures (including the NEM carrier transport). In Sec. III stationary ballistic transport in FET channels is considered, including a simplified analytical treatment. It allows us to analyze a channel current for different values of potentials  $V_D$  and  $V_G$ . In Sec. IV we examine the stability of the obtained stationary solutions and consider the development of current instabilities in the NEM ballistic FET. In Sec. V a model and a procedure of numerical simulations are briefly described. The results of these simulations are presented in Sec. VI. Calculations of the source current dependence on  $V_D$  and  $V_G$  are presented first. These currents are almost free of very high frequency oscillations. Next, gate oscillation

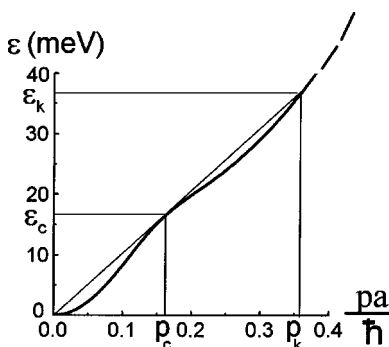


FIG. 2. Dispersion relation  $\varepsilon = \varepsilon(p)$  for the ground quantized hole subband in 8 nm square  $p$ -type GaAs/AlAs quantum well selected as the FET channel and used for numerical simulations;  $a$  is the lattice constant. [Energy interval (0, 250 meV) is really considered for our simulation].

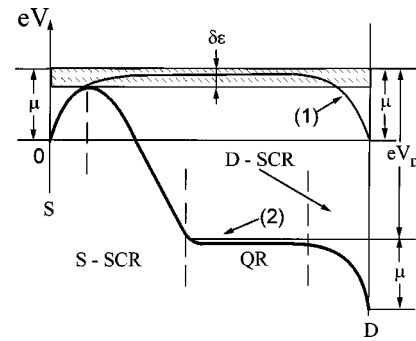


FIG. 3. Distribution of electric potential in the channel for equilibrium (1) and for biasing voltage  $|V_D| \gg \delta\varepsilon$  (2).

currents dependent on stationary values of the same potentials are considered. A brief discussion of some results is presented in Sec. VII, and concluding remarks are in Sec. VIII.

## II. BALLISTIC CARRIER TRANSPORT IN DIODE STRUCTURES

It is known,<sup>1</sup> that ballistic transport of current carriers in a sufficiently long diode base forms a QR in its middle part. The mobile carrier charge is compensated in the QR by the dopants, leading to a mobile carrier concentration,  $N$ , equal to the concentration of ionized donors or acceptors,  $N_A$ , that is  $N = N_A$ . This carrier concentration  $N$  can be written in turn as the sum of the concentrations of ballistic carriers, injected from the source (that is, the cathode in the  $n^+nn^+$  diode or the anode of the  $p^+pp^+$  diode),  $N_1$ , and the concentration of carriers, injected from the drain,  $N_2$

$$N = N_1 + N_2. \tag{1}$$

We assume that transport of both source-emitted carriers and drain-emitted carriers is fully ballistic, and these carriers do not exchange energies or momenta and move in electric fields independently. We also assume, for qualitative consideration, that a sufficiently high voltage  $V_D$  drops across the base. The energy range,  $\delta\varepsilon$  (see Fig. 3), in which there are ballistic carriers, is assumed to be narrow in comparison with  $eV_D$ ,  $\delta\varepsilon \ll eV_D$ . Then the source-emitted carriers can be considered a monoenergetic beam with momentum  $p(x)$ , energy  $\varepsilon(x) = \varepsilon[p(x)]$  and velocity  $v(x) = d\varepsilon/dp|_{p=p(x)}$ . The drain-emitted carriers cannot enter the long source-adjacent spatial charge region (S-SCI, see Fig. 3), and there  $N \approx N_1$ . A one-dimensional (1D) Poisson equation in this region can be written in the form

$$\frac{dE}{dx} = \frac{e}{\kappa_D} \left( \frac{I}{ev(x)} - N_A \right), \tag{2}$$

where  $E$  is an electric field strength,  $\kappa_D$  is a dielectric constant, and  $I$  is a current density

$$I = ev(x)N_1. \tag{3}$$

Assuming a carrier transport is classical, we have

$$\frac{dp}{dx} = \frac{eE}{v(p)} \tag{4}$$

and from Eqs. (2) and (4)

$$e\kappa_D \frac{d(E^2/2)}{dp} = I - ev(p)N_A. \quad (5)$$

[In fact, we have assumed in Eqs. (2) and (4) that the ballistic carriers are holes, but Eq. (5) is independent of this assumption.] Integrating Eq. (5) within the S-SCR with a constant dopant density  $N_A$ , we obtain the following expression, which is acceptable on the border of the S-SCR and the QR (where  $E=0$ ):

$$Ip_1 - e\varepsilon(p_1)N_A = 0, \quad (6)$$

where  $p_1$  is the ballistic carrier momentum in the QR. Equation (6) in combination with Eq. (3) give us the following for the QR:

$$\frac{N_1}{N_A} = \frac{\varepsilon(p_1)}{p_1 v(p_1)}. \quad (7)$$

If  $\varepsilon(p) = p^2/2m$ , and  $v(p) = p/m$ , where  $m$  is a constant effective mass, we find from Eq. (7):

$$N_1 = N_2 = N_A/2, \quad (8)$$

that is, half of the carriers in the QR are ballistic current-conducting (traversing) source-emitted carriers, and the other half are current nonconducting (nontraversing) carriers, that are in equilibrium with the drain carrier reservoir. Taking nonparabolicity of the dispersion relation into account leads to an increase in the share of traversing ballistic carriers  $N_1$  because their effective mass rises. If there is a NEM section in the dispersion relation (see Fig. 2), a certain threshold value of momentum exists. This is  $p = p_c$ , for which  $\varepsilon(p_c) = p_c v(p_c)$ , and  $N_1 = N_A$ ,  $N_2 = 0$ . That is, only traversing ballistic carriers are in the QR. As a result the QR is effectively united with the S-SCR (left in Fig. 3). Further increase in the drain voltage now broadens the drain-adjacent SCR (D-SCR, right in Fig. 3). As long as the QR exists (despite this broadening) the current is saturated:

$$I = I_c = ev_c N_A, \quad (9)$$

where  $v_c = v(p_c)$ . We note that velocity  $v_c$  falls inside the range of velocities corresponding to the NEM section in Fig. 2. This means that only NEM carriers exist in the QR for  $V_c < V < V_k$ . Such NEM plasma is convectively unstable. This instability is globalized (for a diode that has a finite, but sufficiently large size base and is shorted or closed on a small load resistance) and leads to the self-organization of certain oscillatory regimes.<sup>2,3</sup> The oscillations depend on the base length,  $l$ , the doping concentration,  $N_A$ , the load resistance, etc.

We note that the lack of equilibrium (drain-emitted) carriers in the QR (in the presence of ballistic NEM carriers) obviates the problem of momentum and energy transfer due to carrier-carrier interaction. Therefore, our conclusion about the unstable ballistic regime for carriers with the NEM section in the dispersion relation can be extended to high carrier concentration cases where this interaction cannot in principle be neglected.

### III. BALLISTIC CARRIER TRANSPORT IN GATED STRUCTURES

We now consider a hypothetical planar structure [Fig. 1(a)] placed completely between two metallic gates with the same potential  $V_G$ . It is assumed that the distance,  $d$ , between a current-conducting ( $n^+nn^+$  or  $p^+pp^+$ ) channel and each of the gates is small in comparison with the base length,  $l$ , and also with some other lengths characterizing a longitudinal carrier distribution in the base. Then the local potential difference between the gates and some point  $x$  in the base channel defines the local gate charge. Consequently, it controls carrier concentration at that point. We would like to obtain an expression analogous to Eq. (7) for a concentration of current-conducting source-emitted ballistic carriers in the channel QR. (The QR is formed in the middle section of the gated base as before.) With this aim, we use a two-dimensional Poisson equation [instead of one-dimensional Eq. (2)]

$$\frac{\partial E_x}{\partial x} + \frac{\partial E_y}{\partial y} = \frac{e}{\kappa_D} (N - N_A) \delta(y), \quad (10)$$

where  $\delta(y)$  is a Dirac delta-function,  $N$  and  $N_A$  are carrier (hole) and doping (acceptor) concentrations, respectively, in the channel ( $\text{cm}^{-2}$ ; that is, these values differ from bulk concentrations with the same designations introduced in Sec. II). As a result of the integration over the  $y$  coordinate from  $-d$  to  $d$  we obtain

$$\kappa_D^* d \frac{dE_x(0)}{dx} - \frac{2\kappa_D}{d} [V_G - V(x)] = e(N - N_A), \quad (11)$$

where  $E_x(0)$  is a longitudinal field in the channel,  $V(x)$  is a potential of the channel in the point  $x$ , and  $\kappa_D^*$  is defined by an expression

$$\kappa_D^* = \kappa_D \int_{-d}^d E_x dy / E_x(0) d.$$

If a linear decrease of  $E_x(x, y)$  from  $E_x(0)$  in the channel to 0 in the gates takes place  $E_x(x, y) = E_x(x, 0)(1 - |y|/d)$ , we have  $\kappa_D^* = \kappa_D$ . Taking into account (as above) formula (3) and assuming that  $V(p_1) \cong -\varepsilon(p_1)/e$ , where  $V(p_1)$  is a potential of the channel QR, we obtain, analogously to Eq. (7)

$$\frac{N_1}{N_{\text{Ch}}} = \frac{\varepsilon(p_1)}{p_1 v(p_1)} \times \frac{1 - \varepsilon(p_1)/\varepsilon_A}{1 - 2\varepsilon(p_1)/\varepsilon_A}. \quad (12)$$

Here  $\varepsilon_A = e^2 d N_A^* / \kappa_D$ ,  $p_1$  is a carrier momentum in the QR,

$$N_A^* = N_A - \frac{2V_G \kappa_D}{ed}, \quad (13)$$

$N_{\text{Ch}} = N_A^* (1 - 2\varepsilon(p_1)/\varepsilon_A)$  is a total hole concentration in the channel QR. Formally formula (12) reduces to Eq. (7) for  $d \rightarrow \infty$ , when  $N_{\text{Ch}} \rightarrow N_A^* \rightarrow N_A$ , and  $\varepsilon_A \rightarrow \infty$ .

In the parabolic dispersion case,  $\varepsilon(p) = p^2/2m$ , where  $m$  is a constant effective mass, we obtain

$$\frac{N_1}{N_{\text{Ch}}} = \frac{1}{2} \times \frac{1 - \varepsilon(p_1)/\varepsilon_A}{1 - 2\varepsilon(p_1)/\varepsilon_A}. \quad (14)$$

We see that  $N_1 = N_{\text{Ch}}$  if  $\varepsilon(p_1)/\varepsilon_A = 1/3$ . This condition coincides with the saturation of the drain current for such a dis-

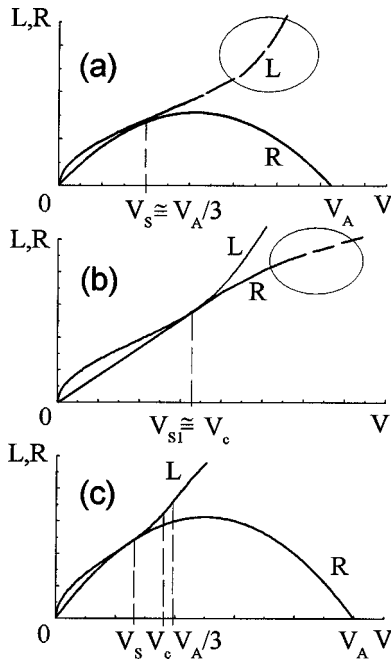


FIG. 4. Finding of saturation voltage  $V_S$  in the point of tangency of the left (L) and right (R) sides of Eq. (15). (a)  $V_A/3 \ll V_c$ . (b)  $V_c \ll V_A/3$ . (c) A case of comparable  $V_A/3$  and  $V_c$ .

persion relation. All of the carriers in the QR become traversing ballistic holes. Holes that are in equilibrium with the drain reservoir are absent. The excess of the drain voltage  $V_D - V_S$ , where  $V_S = -\epsilon_A/3e$  is a saturation voltage, drops across a drain-adjacent depletion region. Analogous results are presented in Refs. 8 and 9 for the ballistic FETs, which have a more complicated design. Nonparabolicity of the dispersion relation decreases the saturation voltage  $V_S$  and saturation current  $I_S$  for given values of  $\epsilon_A$  and  $N_A^*$  (in comparison with a parabolic dispersion relation with the same effective mass at  $p \rightarrow 0$ ). The presence of a NEM section in the dispersion relation lowers these values even more. We can find these values with the help of an equation

$$\lambda p(eV) = V(1 - V/V_A), \tag{15}$$

where  $V = \epsilon(p_1)/e$ ,  $V_A = \epsilon_A/e$ ,  $\lambda = I/e^2 N_A^*$ , and the function  $p(eV) = p(\epsilon)$  is obtained by inverting the dispersion relation of channel carriers  $\epsilon = eV = \epsilon(p)$ . Equation (15) is derived by substituting  $N_1$  from Eq. (12) into Eq. (3). It gives a  $IV$  characteristic of a FET with the QR in the channel. Values  $V(\lambda)$  for given  $\lambda$  can be obtained as abscissas of the intersection point of  $\lambda p(eV)$  with parabolas  $V(1 - V/V_A)$ . Only the first intersection point of two, whose value of  $V$  is smaller, has physical meaning. The saturation case with current  $\lambda = \lambda_S$  corresponds to tangency of curves  $\lambda_S p(V)$  and  $V(1 - V/V_A)$ . A condition of tangency is  $(1 - 2V/V_A)/(1 - V/V_A) = (V/p)(dp/dV)$  and coincides with condition  $N_1 = N_{Ch}$ . The tangency is shown in Fig. 4(a) for a limiting case when  $\epsilon_c \gg \epsilon_A$ , where  $\epsilon_c$  is a characteristic energy that defines the position of the NEM section in the dispersion relation (Fig. 2). In this case the NEM section is not reached, and around the tangency point  $p(eV)$  can be approximated by the parabola  $p(eV) \approx (2emV)^{1/2}$ . As a result, we have

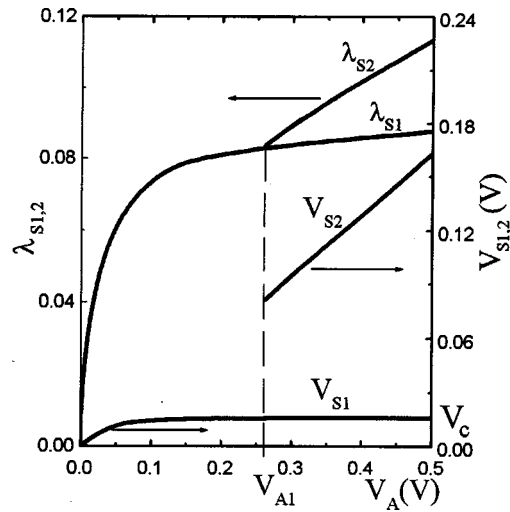


FIG. 5. Saturation voltages  $V_{S1,2}$  and dimensionless saturation currents  $\lambda_{S1,2}$  vs parameter  $V_A$  calculated on the basis of Eq. (15) and the dispersion relation in Fig. 2.

$V_S \approx V_A/3$  and  $I_S \approx 1/3 [(2/3)(d/m) N_A^{*3}]^{1/2}$ . The opposite limiting case when  $\epsilon_c \ll \epsilon_A/3$  is demonstrated in Fig. 4(b). Then the saturation current of the FET is much smaller because this saturation is completely defined by the NEM section in the dispersion relation. This case is the most interesting from our point of view because it leads to a real gate-controlled ballistic NEM diode. For a diode gated in this way we can neglect the second term on the right side of Eq. (12) and consider regime with  $\epsilon_S = p_c v(p_c)$  and  $N_1 = N_A^*$  (that is, with pure NEM plasma). But the value of  $N_A^*$  is set by not only the doping but is additionally controlled by the gate potential.

The value of  $\epsilon_A/3$  is decreased with decreasing  $N_A^*$  and nears  $\epsilon_c$ . As a result a regime of ‘‘combined’’ saturation appears. The concentration of the traversing ballistic carriers in the QR becomes smaller than  $N_A^*$ . We note also that the value of  $V_S$  is smaller for the combined saturation regime than both  $\epsilon_A/3e$  and  $\epsilon_c/e$ . This case is illustrated in Fig. 4(c).

It is easy to ascertain that in the case represented in Fig. 4(b) there are two saturation sections in the  $IV$  characteristic. The first is characterized precisely by the value  $V_{S1} \approx \epsilon_c/e$  and occurs with a smaller saturation current  $\lambda_{S1}$ . The second is characterized by a greater value  $V_{S2}$  that asymptotically approaches  $\epsilon_D/3e$  (if the parabolic relation  $\epsilon = p^2/2m(\infty)$  is reestablished at large values of  $p \gg p_c$  with an effective mass  $m(\infty) > 2m$ ). These two saturation sections appear beginning with a certain value of  $V_A$  that is significantly larger than  $3V_c$ . The saturation voltages  $V_{S1}, V_{S2}$  and relating currents  $I_{S1}, I_{S2}$  are plotted against  $V_A$  in Fig. 5. They are calculated on the basis of Eq. (15) and the particular dispersion relation  $eV = \epsilon(p)$  shown in Fig. 2. (The latter means that the FET channel corresponds to a 8 nm square  $p$ -type GaAs/AlAs QW). We see that  $V_S \approx V_A/3$  for  $V_A \ll 3V_c$  and it is saturated up to  $V_c$  around  $V_A \approx 3V_c$ . The second saturation section appears at  $V_A = V_{A1}$  (see Fig. 5). Here the relationship  $V_{S2} \approx V_A/3$  reappears, while  $V_{S1} \approx V_c$  as before. Since  $V_{A1}$  is noticeably greater than both  $3V_c$  and  $3V_k$ , there is a voltage section where the current increases from

$I_{S1}$  to  $I_{S2}$ . Since the values of  $V_A$ , and as a result  $V_{S2}$  and  $I_{S2}$ , are greater, this section is more extended.

#### IV. INSTABILITY OF THE BALLISTIC PLASMA IN GATED STRUCTURES

We investigate the stability of stationary ballistic plasma in sufficiently long gated structures with QRs and plasma instabilities in the framework of the same model as in Sec. III. All of the dynamic variables are written as sums of stationary values and small nonstationary components. The formers are independent of  $x$  in the QRs. The latter are proportional to  $\exp(ikx - i\omega t)$ , where  $k$  is a real wave number, and  $\omega = \omega(k)$  is a circular frequency, which is generally a complex number and has to be obtained from a dispersion equation. Such a form appears as

$$A(x, t) = A + A'(k) \exp(ikx - i\omega t), \quad (16)$$

where  $A'$  can be  $E'_{xm}, N'_1, N'_2, I'_1, I'_2, p'_1, p'_2, v'_1, v'_2, \varepsilon'_1, V'$ , and the corresponding nonzero values of  $A$  are:  $N_1, N_2, I_1 = I, p_1 = p, v_1 = v(p), \varepsilon_1 = \varepsilon(p), V = \varepsilon/e$ . As before, index 1 relates to traversing carriers, and index 2 relates to nontraversing carriers (which are in equilibrium with the drain carrier reservoir in the stationary case). The following linear equations connect the primed values with each other:

$$\kappa_D \left( ikE'_x + \frac{dE'_y}{dy} \right) - (eN'_1 + eN'_2) \delta(y) = 0, \quad (17)$$

$$ikI'_1 - ie\omega N'_1 = 0, \quad (18)$$

$$ikI'_2 - ie\omega N'_2 = 0, \quad (19)$$

$$I'_1 = evN'_1 + ev'_1N_1, \quad (20)$$

$$I'_2 = ev'_2N_2, \quad (21)$$

$$-i(\omega - vk)p'_1 = eE'_{xm}, \quad (22)$$

$$-i\omega p'_2 = eE'_{xm}, \quad (23)$$

$$\varepsilon' = vp'_1, \quad -ikV' = E'_x, \quad E'_y = -\frac{dV'}{dy},$$

$$v'_1 = p'_1 \frac{d^2\varepsilon}{dp^2} = p'_1/m(p), \quad v'_2 = p'_2/m(0),$$

where  $m(p)$  is an effective mass of traversing carriers (with momentum  $p_1 = p$ ),  $m(0)$  is an effective mass of nontraversing carriers (with momentum  $p_2 \approx 0$ ). Equation (17) follows from the Poisson equation, Eqs. (18) and (20) follow from the equations of continuity of currents  $I_1$  and  $I_2$  (separately), Eqs. (20) and (21) follow from the definition of the ballistic current [see Eq. (3)], and Eqs. (22) and (23) follow from Newton's laws. Equations (18)–(23) allow us to obtain

$$V' - \frac{1}{k^2} \frac{d^2V'}{dy^2} = V'(0) \delta(y) \left( \frac{\Omega_P^2}{\omega^2} - \frac{\Omega_N^2}{(\omega - kv)^2} \right), \quad (24)$$

where  $\Omega_N^2 = -e^2N_1/\kappa_D m(p)$ ,  $\Omega_P^2 = e^2N_2/\kappa_D m$ . (When selecting signs before the right sides of the expressions of  $\Omega_N^2$  and  $\Omega_P^2$  we take into account that the effective mass  $m(p)$  is negative in the case that interests us, and effective mass  $m(0)$

is always positive.) As a result of the solution of Eq. (24) with boundary conditions  $V'(\pm d) = 0$  we obtain a dispersion equation in the form

$$\omega^2(\omega - kv)^2 + \Omega_N^2\omega^2 - \Omega_P^2(\omega - kv)^2 = 0 \quad (25)$$

with

$$\omega_N^2 = \Omega_N^2(k) = \frac{\Omega_N^2 k \tanh kd}{2}, \quad \omega_P^2 = \Omega_P^2(k) = \frac{\Omega_P^2 k \tanh kd}{2}.$$

An analogous equation also occurs for the homogeneously doped bulk diode bases considered in Sec. II. There the frequencies  $\omega_N$  and  $\omega_P$  are independent of  $d$  and  $k$ . They are defined by formulas  $\omega_N^2 = -e^2N_1/\kappa_D m(p)$  and  $\omega_P^2 = e^2N_2/\kappa_D m(0)$ , where  $N_{1,2}$  are bulk concentrations.

If  $\omega_N^2 = 0$  (that is, we have no traversing ballistic carriers, and the plasma consists of nontraversing carriers only), we have

$$\omega_{1,2} = \pm \omega_P; \quad \omega_3 = kv. \quad (26)$$

Frequency  $\omega_P$  defines conventional plasma oscillations of carriers with effective mass  $m(0)$ . The acoustic branch  $\omega_3(k)$  describes excitations to states with velocity  $v$ . If  $\omega_P^2 = 0$  (that is, all of the carriers are traversing), then

$$\omega_{1,2} = kv \pm i\omega_N, \quad \omega_3 = 0. \quad (27)$$

Frequencies  $\omega_{1,2}$  define excitations of the NEM carriers (if  $\omega_N$  is real). The presence of imaginary parts  $\pm i\omega_N$  leads to an infinite increase in the excitation amplitude, making a homogeneous distribution of such carriers unstable. Frequency  $\omega_3 \approx 0$  describes excitations to nontraversing states.

In the general case, when both  $\omega_N^2$  and  $\omega_P^2$  are nonzero and both types of carriers are present, the behavior of the plasma substantially depends on a value of  $kv$ . We introduce a new variable  $s = \omega/k$  and new parameters  $v_{N,P} = \omega_{N,P}/k$ . Then Eq. (25) takes on the form

$$s^2(s - v)^2 + s^2v_N^2 - (s - v)^2v_P^2 = 0. \quad (28)$$

We have  $v_N^2 = -[e^2N_1d/2\kappa_D m(p)](\tanh kd/kd)$  and  $v_P^2 = [e^2N_2d/2\kappa_D m(0)](\tanh kd/kd)$  for the FET structures.

Values  $v_{N,P}$  are constant in the case of  $kd \ll 1$ . They are proportional to  $k^{-1/2}$  if  $kd \gg 1$ , and they are proportional to  $k^{-1}$  if  $\omega_{N,P}$  are constant, as in the bulk diodes. For small values of  $v$  we have two real solutions of Eq. (28)

$$s_{1,2}^2 \approx v^2 \frac{v_P^2}{(v_N \pm v_P)^2}, \quad (29)$$

valid if  $v^2 \ll (v_N \pm v_P)^2$ , and two more solutions

$$s_{3,4} \approx \pm i \sqrt{v_N^2 - v_P^2}, \quad (30)$$

which are imaginary for  $v_N^2 > v_P^2$  and real for  $v_N^2 < v_P^2$ . They are valid if  $v^2 \ll [(v_N \pm v_P)^2/v_P^2] |v_N^2 - v_P^2|$ .

For large values of  $v$  there are two real solutions of Eq. (28)

$$s_{1,2}^2 \approx v_P^2 \left( 1 - \frac{v_N^2}{(v \pm v_P)^2} \right), \quad (31)$$

valid if  $(v \pm v_P)^2 \gg v_N^2$ , and two complex solutions

$$s_{3,4} \cong v \pm i \frac{v v_N}{\sqrt{v^2 - v_p^2}}, \quad (32)$$

valid if  $v^2 - v_p^2 \gg v_N^2$ . If  $v^2 \gg v_p^2$ , solutions (32) are the same as solutions  $\omega_{1,2}$  in Eq. (27) for the case  $\omega_p^2 = 0$ . We see that a homogeneous state of mixed plasma is unstable practically for all of the values of  $kv$  if  $\omega_N^2 > \omega_p^2$ , but it is unstable even if  $\omega_N^2 < \omega_p^2$  for large values of  $kv$ , as it can be deduced from formula (32).

We see that the homogeneous plasma section (the QR) in the gated FET structures is as unstable as in the ungated diode bases. But in realistic structures this section is included in series with the SCRs. Therefore, the problem of globalization of the above mentioned instabilities and self-organization of oscillatory regimes requires additional detailed analysis. This problem is considered below by means of numerical simulations of selected FET structures.

### V. NUMERICAL SIMULATION PROCEDURE

The design selected for our numerical simulations [Fig. 1(b)] differs substantially from the simplified design of Fig. 1(a), and seems more realistic. There is a single top gate, and it is of a finite size. A source and a drain are brought out from under the gate, and some clearances (with size  $c$ ) appear between the gate and the source, as well as between the gate and the drain. The active region is confined by drain and source quasimetallic planes on the sides. On the top and bottom planes we impose periodic boundary conditions. That is, we consider an infinite system of parallel gated channels instead of a single channel. Spatial period  $2b$  is assumed large enough to consider each of them as approximately independent. (Behavior of such spatially periodic  $p^+pp^+$  diode structures that depends on  $2b$  is described in detail in Ref. 5).

We assume that current flows only in the current-conducting channel. Therefore, we have a one-dimensional ballistic transport problem. Distribution functions of carriers entering the channel from the drain and the source are specified in the form of Fermi-Dirac functions with given Fermi energies  $\mu$ . The electric fields exist everywhere, but mainly in the barriers outside the channel. As a result, the Poisson problem is two dimensional. It has to be solved for the given source ( $V_{SR} = 0$ ), drain ( $V_D$ ) and gate ( $V_G$ ) potentials. We restrict ourselves to the Poisson equation and do not take into account magnetic fields. This formulation of the problem seems reasonable for our confined spatially periodic structure, which cannot radiate electromagnetic waves into free space. (This structure allows us to withdraw oscillation power only by means of an electric load in the drain circuit.) The self-consistent solution of the Poisson equation and the ballistic kinetic equation is obtained analogously to our treatment of ungated  $n^+nn^+$  and  $p^+pp^+$  diodes with current-conducting channels described in detail in Ref. 6. To obtain detailed information about the current oscillations we assume that one of the two potentials,  $V_D$  or  $V_G$ , is fixed, while the other is assumed to be increasing or decreasing slowly with time

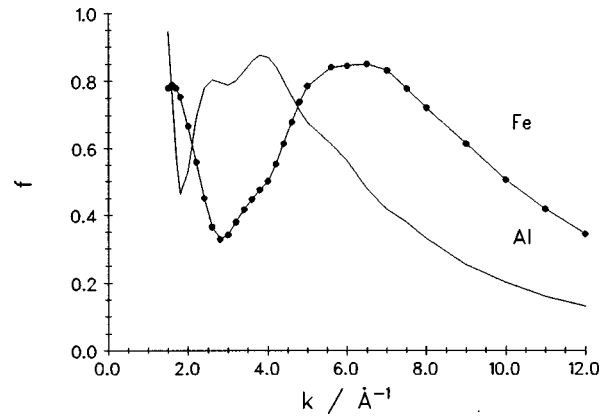


FIG. 6. Source current  $I_{SR}$  vs drain-source voltage  $|V_D(t)|$  and time  $t$  for the selected FET design.  $V_G = 0.05$  V (1), 0.025 V (2), 0 (3),  $-0.025$  V (7),  $-0.05$  V (8),  $-0.075$  V (9),  $-0.10$  V (10),  $-0.125$  V (11). Voltage  $V_D(t)$  changes with time [Eq. (33)] with the rate  $V'_D = 0.002$  V/ps. Characteristic (11) is shifted upward 0.05 A/cm.

$$V_{D,G}(t) = V_{D,G}(0) + V'_{D,G}t. \quad (33)$$

This procedure, when used for the stable quasistationary regime with adiabatically small rates  $V'_{D,G}$ , allows us to measure either  $I_D = I_D(V_D)$  for a given  $V_G$  or  $I_D = I_D(V_G)$  for a given  $V_D$ . In both cases, the drain current  $I_D$  is equal to source current  $I_{SR}$ , and these currents flow entirely through the channel. If we have an oscillatory regime, this procedure allows us to observe the portrait of the oscillations (as a function of time) through the background of  $IV$  characteristics. We can evaluate the fundamental frequency, amplitude, and harmonic composition of oscillations for different  $V_G$  and  $V_D$ . Because of displacement currents, now  $I_D \neq I_{SR}$ , and a gate current  $I_G = I_D - I_{SR}$  does exist. We calculate currents  $I_D$  and  $I_{SR}$  as full currents through certain planes. These planes  $ss'$  and  $dd'$  are parallel to the drain (source) plane and are placed between the gate and the drain or the source, respectively [see Fig. 1(b)].

We assume for simplicity that the channel is directly doped with acceptors (but we keep in mind that modulation doping will really be implemented to provide the ballistic carrier transport in the channel).

### VI. RESULTS OF SIMULATIONS

The design, which we selected for simulation [Fig. 1(b)], is described by the following set of numbers:  $l = 0.2 \mu\text{m}$ ,  $l_G = 0.16 \mu\text{m}$  (that is,  $c = (l - l_g)/2 = 0.02 \mu\text{m}$ ),  $2b = 0.16 \mu\text{m}$ , a distance gate-channel  $d = 0.016 \mu\text{m}$ ,  $N_A = 10^{11} \text{cm}^{-2}$ ,  $\mu = 10 \text{meV}$  (this value is the same both for the drain and for the source),  $\kappa_D = 10.9$  (as in AlAs), temperature  $T = 4.2 \text{K}$ . Rates  $V'_{D,G}$  in Eq. (33) are selected to be equal to 0.2 mV/ps. We select for our simulation the dispersion relation of quantized holes presented in Fig. 2 because in this case the NEM range extends up to  $\epsilon_c \cong 0.035 \text{eV}$ , lower than the optical phonon energy in GaAs (0.036 eV). Therefore, the channel holes in the NEM range cannot emit such phonons and stay ballistic.

The source current  $I_{SR}$  as a function of time in our model FET is presented in Fig. 6 for  $V_D$  that increases with time

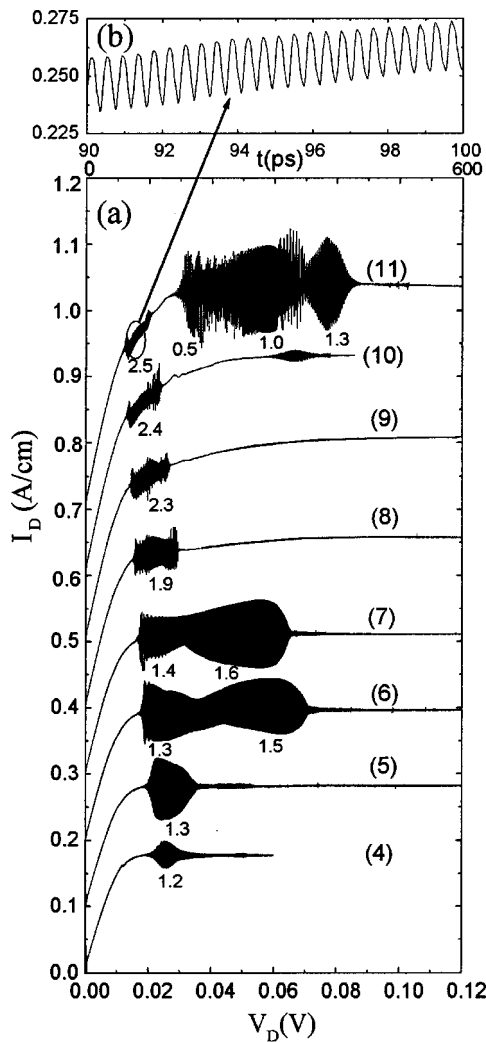


FIG. 7. (a) Drain current  $I_D$  vs drain-source voltage  $|V_D(t)|$  and time  $t$  for the same FET design.  $V_G = -0.004$  V (4),  $-0.008$  V (5),  $-0.016$  V (6),  $-0.025$  V (7),  $-0.05$  V (8),  $0.075$  V (9),  $-0.10$  V (10),  $-0.125$  V (11). Characteristics are shifted upward relative to each other  $0.1$  A/cm. Numbers near characteristics are oscillation frequencies (THz) in nearby sections. (b) Fragment of characteristic for  $V_G = -0.125$  V.

according to Eq. (33) and eight values of  $V_G$  from  $+50$  mV to  $-125$  mV. The characteristics for  $V_G = 50, 25,$  and  $0$  mV remind us of characteristics of the conventional FET, and do not contain any oscillations. But all of the characteristics for negative  $V_G$  exhibit oscillatory phenomena with oscillations becoming very significant for  $V_G = -125$  mV. Figure 7 (where the analogous characteristics of the drain current  $I_D$  are presented) and Fig. 8 (where the gate current  $I_G = I_D - I_{SR}$  oscillations are shown) confirm these results very convincingly. As mentioned above, amplitudes of  $I_D$  and  $I_G$  oscillations are much greater than  $I_{SR}$  oscillation amplitudes. In Figs. 7 and 8 we present characteristics of  $I_D$  and  $I_G$  for several small enhancing values of  $V_G$  ( $-4, -8, -16$  mV). Current oscillations can be observed starting with  $V_G = -2$  mV. For  $V_G = -4$  mV we see very noticeable oscillations of the gate and drain currents in the range of  $V_D = 15\text{--}35$  mV. These oscillations are distinctly sinusoidal with frequency  $\sim 1.2$  THz. Increasing the negative values of  $V_G$  results in broadening of the  $V_D$  range of oscillations. It also shifts the

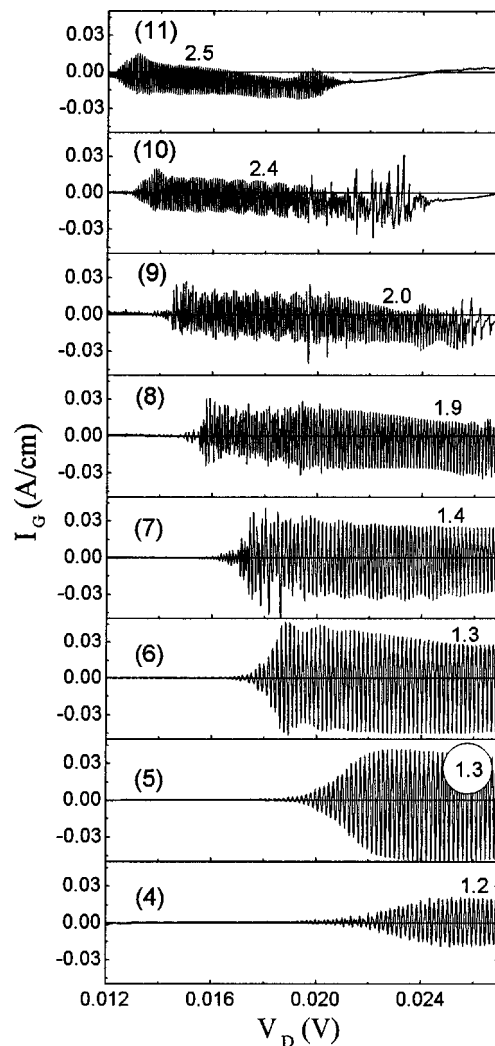


FIG. 8. Gate current  $I_G = I_D - I_{SR}$  vs drain-source voltage  $|V_D(t)|$  and time  $t$  for the same gate potentials as in Fig. 7(a). The extended time scale allows us to examine oscillation shape and to estimate frequency. Numbers near characteristics are oscillation frequencies (THz) in nearby sections.

maximum oscillation amplitudes towards higher  $V_D$  values (see  $I_D(V_D)$  in Fig. 7 for  $V_G = -8, -16,$  and  $-25$  mV). For example, for  $V_G = -25$  mV the maximum oscillation amplitude is reached at  $V_D \approx 55$  mV, and the  $V_D$  range of oscillations is  $16\text{--}65$  mV. Amplitudes of the drain and gate current oscillations exceed amplitude of source current oscillations by a factor of  $30\text{--}40$ . Increasing  $V_G$  further narrows the  $V_D$  range of oscillations on the account of the high-voltage part. These  $V_D$  ranges for  $V_G = -50, -75, -100,$  and  $-125$  mV exist only in the restricted NEM limits, and, naturally, oscillations in these ranges are related to the NEM instability. We note that the average current in the NEM sections for  $V_G = -75, -100,$  and  $-125$  mV is far from saturated and rises very noticeably. It is worth noting<sup>2,5,6</sup> that in the case of ungated planar channel bases the strict saturation also does not occur. But in the FETs this current rise seems far greater.

The most noticeable feature of the NEM oscillatory regimes in ballistic NEM FETs is a monotonic rise in oscillation frequency with increase in enhancing gate potential: from  $f = \omega/2\pi \approx 1.2$  THz for  $V_G = -4$  mV to  $f \approx 2.5$  THz for  $V_G = -125$  mV. This increase can also be monitored in Fig.

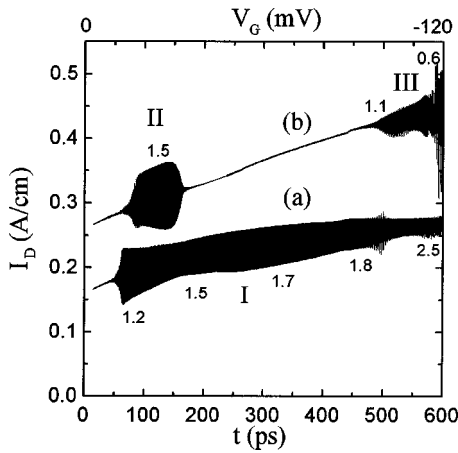


FIG. 9. Drain current  $I_D$  vs gate potential  $V_G(t)$  and time  $t$ .  $|V_D| = 0.018$  V (a) and  $0.055$  V (b). Characteristic (b) is shifted upward  $0.1$  A/cm. (I) Area of the 1st type oscillations. (II) Area of the 2nd-type oscillations. (III) Area of the 3rd-type oscillations. Numbers near characteristics are oscillation frequencies (THz) in nearby sections.

9 where characteristics  $I_D = I_D(V_G)$  are presented for two values of  $V_D$ ,  $V_D = -18$  and  $-55$  mV. The former is in the NEM section, and the frequency rises monotonically with the current. This rise is accompanied by decreasing amplitudes for high values of  $V_D$ .

For  $V_G = -100$  mV the second oscillatory range appears unrelated to the above-described NEM section. Oscillation frequencies in this section are much lower than in the NEM section. These oscillations take place through the background of well-marked FET current saturation (that is due to the gate effect). At  $V_G = -125$  mV the second oscillatory section becomes significantly wider. In contrast to the NEM oscillation these oscillations are present not only in the drain and gate currents but also in the source current. This distinctive peculiarity cannot be explained only by pronounced difference between oscillation frequencies for these ranges. Oscillation frequencies ( $\sim 1$  THz) for  $V_G = -4$  and  $-8$  mV are of the same order as in the second section for  $V_G = -125$  mV but they are not manifested in the source current for the former and are manifested for the latter. This gives evidence of the different origin of current oscillations for large values of  $V_D$  in these two cases.

Let us turn to the  $I_D = I_D(V_G)$  characteristic for  $V_D = -55$  mV (Fig. 9). We can see here two oscillation ranges, which are isolated from each other by a large gate voltage gap. The source current oscillations are presented only in the high  $V_G$  range.

To diagnose current oscillations, which appear in different areas of  $\{V_D, V_G\}$  plane we consider nonstationary concentration and potential distributions in the FET channel. We discover three typical oscillation signatures illustrated in Fig. 10. The first of them [Fig. 10(a)] appears at small values of  $V_D$  and is due to the NEM instability [ $V_D = -(15-35)$  mV]. This range shifts to smaller voltages with increasing values of  $V_G$ . The picture is very much like that of ungated diode generators.<sup>6</sup> The spatial charge wave consisting of alternating layers of accumulation and depletion originates under the gate and drifts to the drain while rising in the amplitude. The

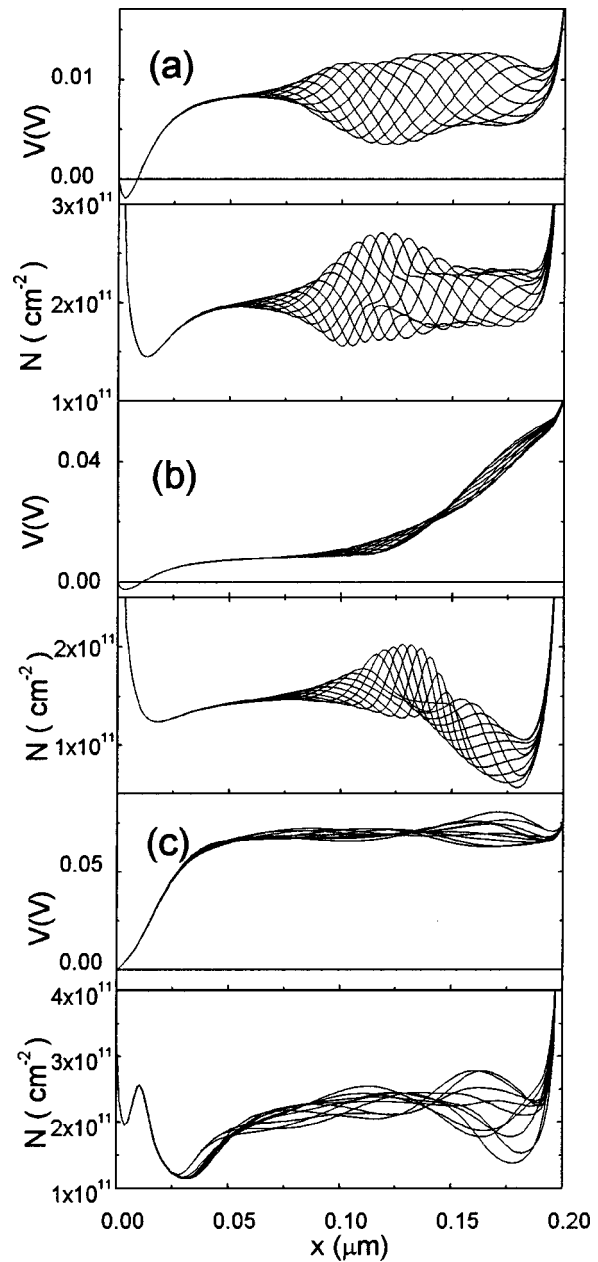


FIG. 10. Pictures of concentration and potential oscillations for three types of oscillatory regimes. (a) Oscillations of the 1st type ( $V_G = -0.050$  V,  $|V_D| \cong 0.020$  V). (b) Oscillations of the 2nd type ( $V_G = -0.025$  V,  $|V_D| \cong 0.055$  V). (c) Oscillations of the 3rd type ( $V_G = -0.125$  V,  $|V_D| \cong 0.080$  V).

left side of the base is not affected and therefore the source current oscillations are absent. Increasing the enhancing gate voltage and hence the channel carrier concentration results in a decrease of the effective oscillation wavelength and, as a result, of oscillation frequency.

The second type of oscillation [Fig. 10(b)] takes place for comparatively small gate potentials  $V_G$  and large drain potentials  $V_D \gg V_k \cong \epsilon_k/e$  (Fig. 2). It corresponds to the oscillation area II in characteristic  $I_D = I_D(V_G)$  for  $V_D = -55$  mV in Fig. 9. In this case the current is saturated (as in conventional FETs), and the voltage of saturation,  $V_S$ , is in the NEM limits. (We remember that all the excess of the drain voltage over the voltage of saturation,  $V_D - V_S$ , drops

on the depletion region adjacent to the drain. This region widens with increase in  $V_D$  but a channel potential on the left side of the depletion layer stays constant.) As a result we obtain intensive NEM oscillations in the channel QR for drain voltages  $V_D$ , which are much greater than  $V_k \equiv \varepsilon_k/e$ . These oscillations also perturb the concentration and potential distributions in the depletion region. They can exist only in the narrow range of gate potentials because the voltage of saturation  $V_S$  has to be within the strictly determined limits.

The third type of oscillation occurs at large both  $V_G$  and  $V_D$  values. In this case the saturation voltage of our gated diode (as for the conventional FET) is greater than  $V_k \equiv \varepsilon_k/e$ , and the entire NEM section of the dispersion relation is hidden in the left (source-adjacent) spatial charge region. Oscillations develop in the QR where NEM carriers are absent completely. A region of oscillations includes almost all the space under the gate. There appear significant oscillations of the source current, which are negligible in the previous cases. Such a picture reminds us of development of the two-stream instability. This phenomenon does not, in principle, require a NEM section in the dispersion relation. But it also differs from the standard picture for the FETs, which have channel carriers with the parabolic dispersion relation.

## VII. DISCUSSION

The results of numerical simulations described in Sec. VI confirm for the most part our analytic forecasts. Some discrepancies can be attributed to incomplete similarity of the designs shown in Figs. 1(a) and 1(b). The oscillatory regime of the second type [Fig. 10(b)] initiated by the shortened NEM plasma QR, which is separated from the drain by the wide depletion region, is similar to the analogous regime described in Ref. 5 for ungated  $p^+pp^+$  diodes. The upper limit of the drain voltage range of oscillations in Ref. 5 significantly exceeds the  $V_c = \varepsilon_c/e$  limit that occurs only in the regime of the first type [Fig. 10(a)]. The most unexpected results relate to the third type of the oscillation [Fig. 10(c)], which we attribute to the development of a two-stream instability.<sup>11</sup> Development of the two-stream instability has repeatedly been predicted for ballistic diodes with a parabolic dispersion relation (see Refs. 12, 13 and therein). But this instability cannot exist if a current is saturated because in this case the only carrier stream (of traversing holes) takes place in the channel QR ( $N_1 = N_{Ch}$ , and  $N_2 = 0$ ). To confirm this fact  $I_D(V_D)$  characteristics of one more FET, which has the same design as in Fig. 1(b), are presented in Fig. 11. Channel carriers in this FET have the simplest dispersion relation  $\varepsilon = p^2/2m$  with the effective mass  $m$  of GaAs heavy holes. The dispersion relation in Fig. 2 asymptotically tends to this relation at  $p \rightarrow \infty$ . We can observe well-developed oscillations only in sections of increasing current. Frequencies of these oscillations increase with negative values of  $V_G$  from 0.5 THz for  $V_G = -50$  mV to 1.4 THz for  $V_G = -125$  mV. Analogous oscillations with smaller amplitudes are present in the source current. But we observe no oscillations in the saturation sections of all of these characteristics. This result completely corresponds to the prediction of Ref. 9.

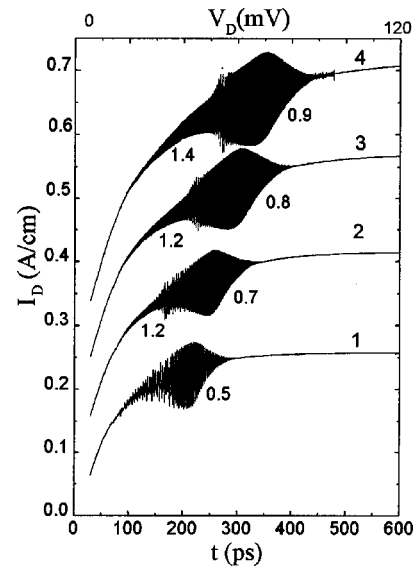


FIG. 11. Drain current  $I_D$  vs drain-source voltage  $|V_D(t)|$  and time  $t$  for the FET having a parabolic dispersion relation of the channel holes:  $m = 0.65m_o$ , where  $m_o$  is the free electron mass.  $V_G = -0.050$  V (1),  $-0.075$  V (2),  $-0.100$  V (3),  $-0.125$  V (4). Characteristics are shifted upward relative to each other 0.1 A/cm. Numbers near characteristics are oscillation frequencies (THz) in nearby sections.

Detailed study of concentration and potential distributions in the ranges corresponding to the third type of oscillation shows that we are dealing with a certain regime of pseudosaturation. Despite the apparent current saturation, the carrier concentration in the channel QR does not stay constant but decreases with increasing  $V_D$ . The source-adjacent depletion region on the left of the QR also does not stay constant and increases. The drain-adjacent depletion region is absent. This means that two groups of carriers coexist in the channel QR:  $N_1 < N_{Ch}$ , and  $N_2 > 0$ . These two groups are responsible for existence of twostream instability. We note that these two groups of carriers substantially differ from two groups considered before both in works<sup>9,12,13</sup> and in our calculations, which are presented in Fig. 11. It is because these carriers are of different effective masses. Ballistic traversing holes have a heavy effective mass (nearing heavy hole mass), and nontraversing holes are much lighter. Therefore, oscillation signatures in this case seem more complicated than for the channel carriers with a parabolic dispersion relation (Fig. 11). The pseudosaturation regime transforms into a real saturation regime at very large values of  $V_D$ . These values are greater for greater values of  $V_G$ .

## VIII. CONCLUDING REMARKS

We have shown that unstable stationary regimes appear in the gated NEM ballistic diodes as in their ungated predecessors. Development of instabilities for these regimes leads to self-organized generation of current oscillations accompanied by concentration and electric field oscillations. These phenomena in the FET variant are displayed in more varied form because gate potentials control both a drain voltage range of the oscillations and the oscillation frequencies. The oscillation frequency in the NEM range rises monotonically with the increase in enhancing gate potential. It more than

doubles as the gate potential is changed from 0 to  $-125$  mV. An advantage of the ballistic NEM FETs is in effective reduction of the length of oscillation region because an oscillating current enters the base channel from the gate (instead of the source). As a result, the oscillation region is shifted significantly to the right, towards the drain and shortens.

Along with the standard regime of NEM oscillations which occurs in the NEM range of drain voltages, the second NEM-oscillatory regime is shown and described for small enhancing gate potentials. It is characterized by larger drain-source voltages (far outside the NEM range). Oscillations in this case are generated in some inner spatial segment of the base where NEM carriers predominate. The excess voltage drops over a depletion segment, which is placed between the above-mentioned segment and the drain.

Besides the NEM oscillations, our simulations reveal oscillations of another nature. They appear at  $|V_G| \geq 100$  mV and are initiated by the two-stream instability. This instability is predicted<sup>9</sup> for ballistic FETs where channel current carriers have a parabolic dispersion relation with a single effective mass. In this case such instability takes place only in a section of  $I_D(V_D)$  characteristic where drain current  $I_D$  rises with drain potential  $V_D$  and does not take place in a current saturation section. Our numerical simulations also demonstrate the generation of current oscillations in the rising current sections and confirm this result. But this result is unusable for nonparabolic dispersion relations considered here. Effective masses of current carriers in interacting beams now are substantially different, and the phenomenon becomes more varied. Specifically, oscillatory regimes developed in the section of visible saturation (pseudosaturation) are displayed. These regimes are of undoubted interest, although oscillation frequencies for the two-stream oscillatory regimes are 2.5–3 times lower than for the NEM regimes at the same gate voltage. This is so because the list of candidate materials for the FET current channels becomes much longer.

Here we have considered only ballistic devices where the channel is completely or almost completely controlled by the gate. But there are possible gated structures where the channel is covered by a gate (or by two gates) only partially. Such devices allow us to design more favorable distributions of carrier concentration and electric field along the current direction and to reach ultimately higher oscillation frequencies. Some results in this direction were presented recently in Ref. 14.

## ACKNOWLEDGMENTS

The authors cordially thank Professor A. Zaslavsky from Brown University for fruitful discussion, Dr. V. Korobov from Ford Motor Corporation for valuable comments, and O. Melnikova for her friendly help. This work was supported by NSF and JPL DFDR grants.

- <sup>1</sup>Z. S. Gribnikov and A. N. Korshak, *Semiconductors* **28**, 812 (1994).
- <sup>2</sup>N. Z. Vagidov, Z. S. Gribnikov, and A. N. Korshak, *Semiconductors* **29**, 1014 (1995).
- <sup>3</sup>N. Z. Vagidov, Z. S. Gribnikov, and A. N. Korshak, *JETP Lett.* **61**, 38 (1995).
- <sup>4</sup>N. Z. Vagidov, Z. S. Gribnikov, and A. N. Korshak, *Semiconductors* **31**, 150 (1997).
- <sup>5</sup>Z. S. Gribnikov, A. N. Korshak, and V. V. Mitin, *Int. J. Infrared Millim. Waves* **20**, 213 (1999).
- <sup>6</sup>Z. S. Gribnikov, A. N. Korshak, and N. Z. Vagidov, *J. Appl. Phys.* **80**, 5799 (1996).
- <sup>7</sup>A. N. Korshak, Z. S. Gribnikov, N. Z. Vagidov, S. I. Kozlovsky, and V. V. Mitin, *Microelectron. Eng.* **43-44**, 445 (1998).
- <sup>8</sup>A. A. Sukhanov, V. B. Sandomirskii, and Yu.Yu. Tkach, *Sov. Phys. Semicond.* **17**, 1378 (1983).
- <sup>9</sup>V. V. Mantrov and A. A. Sukhanov, *Sov. Phys. Semicond.* **19**, 882 (1985).
- <sup>10</sup>Z. S. Gribnikov, A. N. Korshak, and V. V. Mitin, *Proceedings of 24th International Conference on Physics Semicondors* (World Scientific, Singapore, 1998), TH-P93.
- <sup>11</sup>M. V. Nezhlin, *Sov. Phys. Usp.* **11**, 608 (1971).
- <sup>12</sup>V. I. Ryzhii, N. A. Bannov, and V. A. Fedirko, *Sov. Phys. Semicond.* **18**, 481 (1984).
- <sup>13</sup>Z. S. Gribnikov, A. N. Korshak, S. I. Kozlovsky, and N. Z. Vagidov, *Lith. Phys. J.* **36**, 599 (1996).
- <sup>14</sup>A. N. Korshak, Z. S. Gribnikov, N. Z. Vagidov, and V. V. Mitin, *Appl. Phys. Lett.* **75**, 2292 (1999).